Supplemental information

Supplemental legend

Table S1. Identified nociceptor-enriched genes and screen result (related to Figure 1 and 2).
(A) A list of nociceptor-enriched genes. CG number, enrichment in Class IV (Class IV/Class I), p-value with Welch's t-test and synonyms are shown for each gene. (B-E) Initial screen results. VDRC 1st-gen (GD) RNAi lines (B), VDRC 2nd-gen (KK) RNAi lines (C), TRiP RNAi lines (D) and NIG RNAi lines (E). The ID of the RNAi line in each library, and CG number, annotated name, Class IV enrichment of the target gene are included. Average latency, SEM, and the number of larvae tested are separately shown for the insensitivity screen (46 °C) and hypersensitivity screen (42 °C). RNAi lines that fell above the cut-off line for the insensitivity screen are highlighted in orange and RNAi lines that fell below the cut-off line in hypersensitivity screen are highlighted in blue. (F-M) Retest results. Retest results of the insensitive hits from VDRC 1st-gen (GD) RNAi lines (F), hypersensitive hits from VDRC 1st-gen (GD) RNAi lines (G), insensitive hits from VDRC 2nd-gen (KK) RNAi lines (H), hypersensitive hits from VDRC 2nd-gen (KK) RNAi lines (I), insensitive hits from TRiP RNAi lines (J), hypersensitive hits from TRiP RNAi lines (K), insensitive hits from NIG RNAi lines (L) and hypersensitive hits from NIG RNAi lines (M). Lines are listed from strongest to weakest phenotypes in the initial screen. The number of larvae tested, average latency, SEM and p–value when compared to a control score in the retest are shown. The ID of the RNAi line in each library, and CG number, annotated name, Class IV enrichment of the target gene and average latency in the initial screen are also included. RNAi lines whose insensitive and hypersensitive phenotype were retested with statistical significance are highlighted in orange and blue, respectively. (N and O) Results of no driver controls. Positive hit RNAi lines were crossed to w^{1118} strain and tested for the phenotype that was observed in retests when combined with *ppk-GAL4 UAS-dicer2* strain. The number of larvae tested, average latency, SEM and p–value when compared to a control score in the retest are shown.

Supplemental Table

	Annotated site (Empty)	Annotated site (Insertion)	Non-annotated site (Empty)	Non-annotated site (Insertion)
60100 (control)	✓		✓	
KK100198	✓			✓
KK100312		✓		✓
KK100533	✓			✓
KK100573	**?**	**?**		✓
KK101991	**?**	**?**		✓
KK102047	✓			✓
KK105905		✓		✓
KK106169		✓		✓
KK106294	✓			✓
KK107387	✓			✓
KK107503	✓			✓
KK108683		✓	✓	

Table S2. PCR verification of insertion sites for our KK line hits (related to Figure 2).
PCR reactions were carried out to determine the presence or absence of UAS-RNAi insertions at the annotated attP site or the "non-annotated site" according to the methods described in Green et al (2014). Check marks indicate a positive PCR result confirming either the presence of an insertion or an empty attP site. The PCR results were not informative for two of the lines (KK100573 and KK101991) at the annotated site as neither reaction for this site produced a positive PCR result. The uncertainty for the annotated site in these lines are indicated as question marks. Note that insertions at the annotated site have the potential to be problematic due to unintended over-expression of *tio*.

Supplemental figures

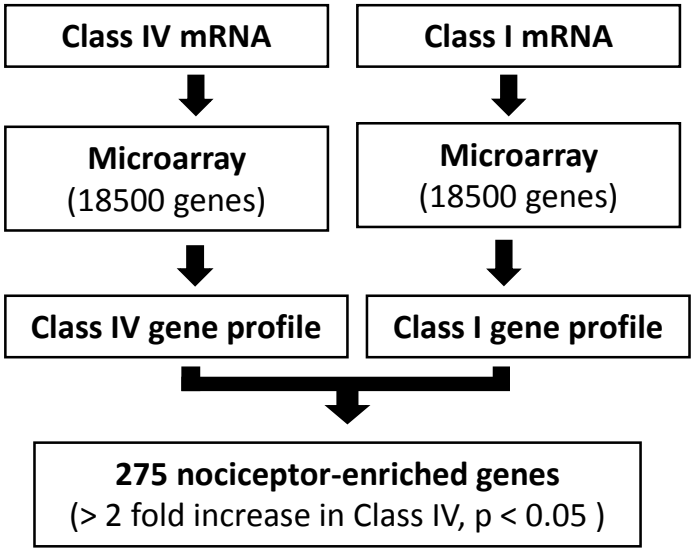

Figure S1. Identification of Class IV enriched genes (related to Figure 1)
A flow chart of the comparative microarray analysis to identify nociceptor-enriched genes. See also Figure1 and Table S1A.

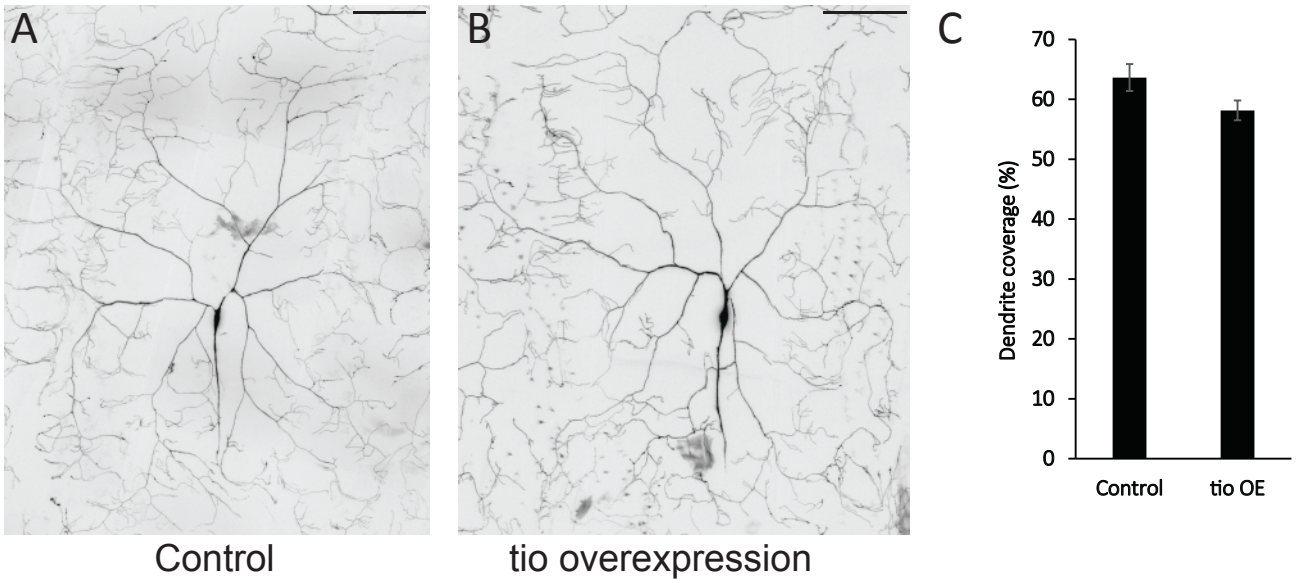

Figure S2. Dendritic morphology of Class IV neurons overexpressing tio gene (related to Figure 4).
(A and B) Representative images of the dendritic structure of ddaC Class IV neurons. Control *(ppk-GAL4 UAS-mCD8::GFP; UAS-dicer2 x* w^{1118}*)* and tio overexpression *(ppk-GAL4 UAS-mCD8::GFP; UAS-dicer2 x UAS-tio)*. Scale bars represent 100 µm.
(C) Quantified dendrite coverage of ddaC Class IV neurons overexpressing tio. No statistical difference was detected in conmarison to control neurons ($p > 0.1$, $n = 7$ and 8, Mann-Whitney's U-test). Error bars represent SEM.

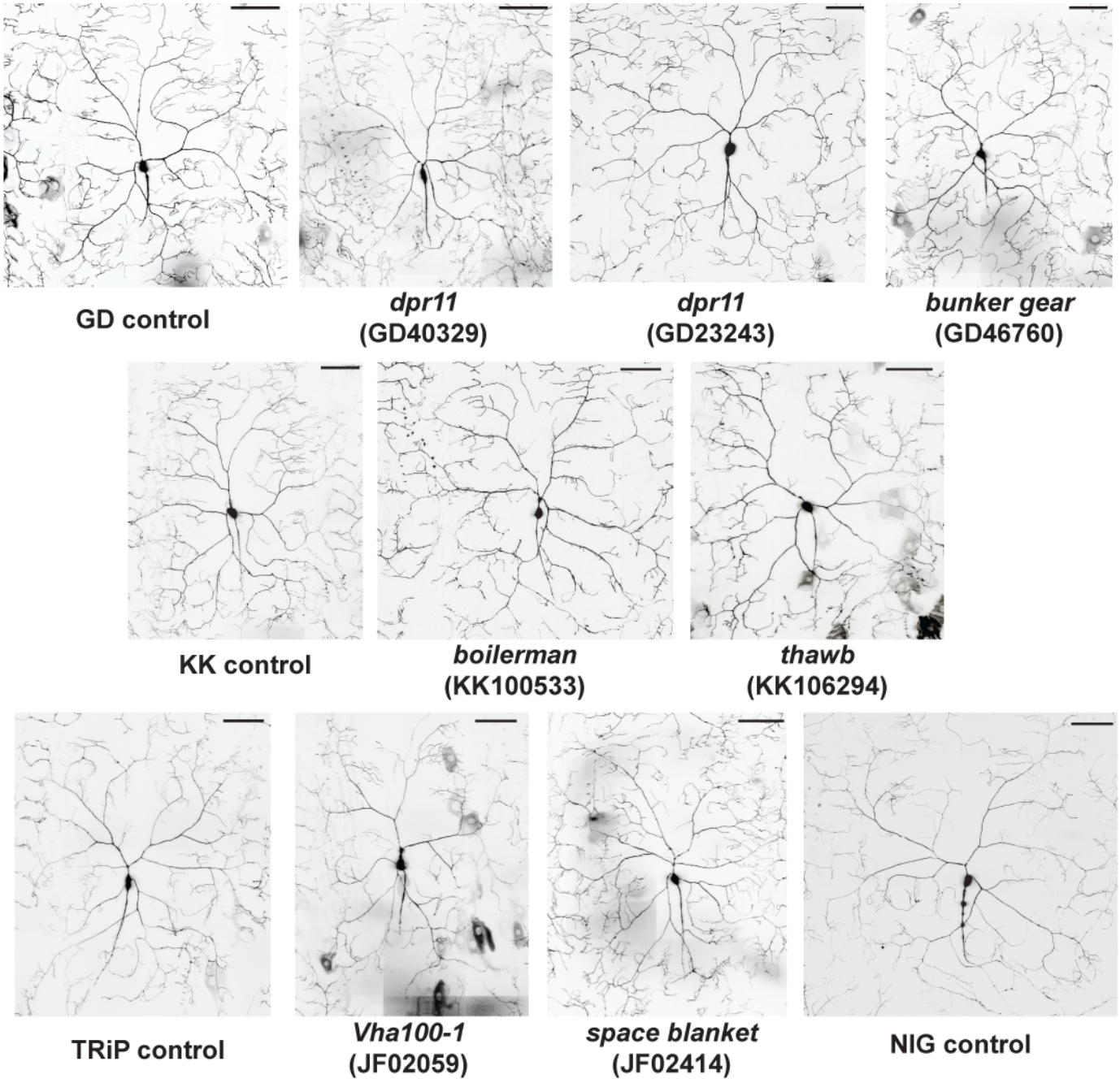

Figure S3. RNAi strains that showed insensitive thermal nociception but unaltered dendritic morphology of Class IV neurons (related to Figure 3). Representative pictures of the dendritic structure of ddaC Class IV neurons in RNAi animals that exhibited insensitive thermal nociception in our screen and control animals. See Figure 3 for quantified data. Scale bars represent 100 μm.

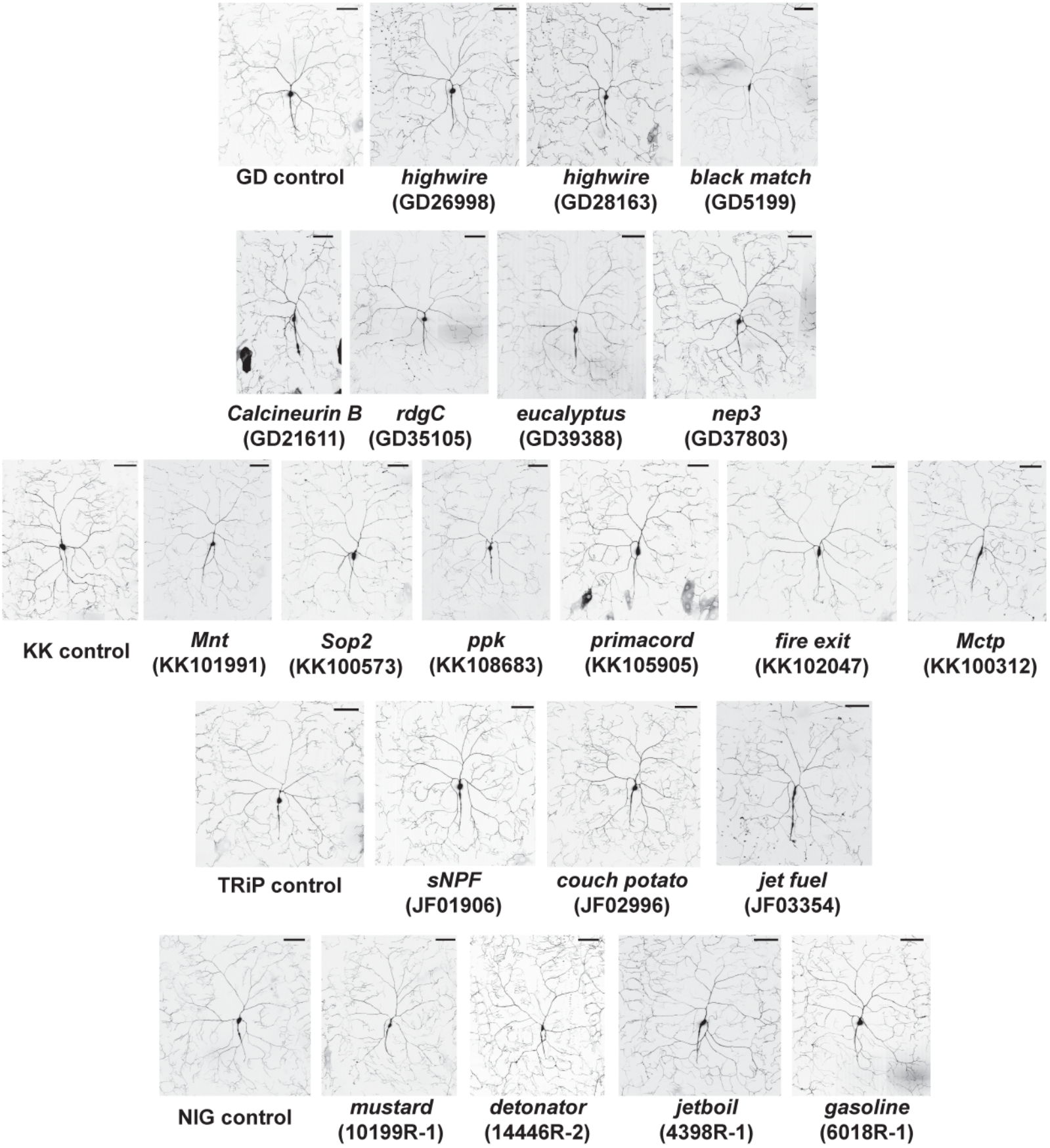

Figure S4. RNAi strains that showed hypersensitive thermal nociception but unaltered dendritic morphology or mild reduction in coverage of Class IV neurons (related to Figure 4).

Representative pictures of the dendritic structure of ddaC Class IV neurons in RNAi animals that showed hypersensitive thermal nociception in our screen and control animals. See Figure 4 for quantified data. Scale bars represent 100 μm.

Supplemental experimental procedures

Fly strains

All UAS-RNAi lines tested in the nociceptor-specific RNAi screen are listed in Table S1B-E. The VDRC provides a computational prediction for the number of possible off-target effects for each line in the collection. As a precaution against off-target effects, we did not include any line with greater than two potential off-targets in our genetic screen. VDRC *isow* line, VDRC 60100, *yv; attP2* and w^{1118} strains crossed to *w; ppk1.9-GAL4; UAS-dicer2* strain were used as controls for VDRC 1st-gen RNAi (GD) lines , VDRC 2nd-gen RNAi (KK) lines, TRiP RNAi lines and NIG RNAi lines, respectively. *ppk1.9-GAL4 UAS-mCD8::GFP; UAS-dicer2* was used for dendrite imaging.

Behavioral experiments

Different sets of larvae were used for 46°C and 42°C tests. In the initial screen, at least 15 larvae were tested for each *UAS-RNAi* x *ppk1.9-GAL4; UAS-dicer2* pair. Average latency to respond to the thermal probe stimulation was calculated and compared to the latency of control crosses. Crossed progeny from driver to RNAi strains that showed significantly longer latency to respond to 46°C probe or shorter latency to 42°C probe than controls were retested. Approximately 45 larvae were tested in the repeated testing round. The latency data for the second round of testing for the progeny of each *UAS-RNAi x ppk1.9-GAL4; UAS-dicer2* cross was compared to pooled latency data of control crosses that were tested side-by-side with the RNAi crosses, and RNAi strains whose phenotype held up were determined as positive hits. Steel's test (non-parametric equivalent of Dunnet's test) was used for the statistical comparisons, except that Mann-Whitney's U-test was used to perform the pair-wise comparison between controls and NC2beta RNAi shown in Figure 2A and 3B.

Dendrite imaging

Each RNAi line was crossed to *ppk1.9-GAL4 UAS-mCD8::GFP; UAS-dicer2*. Wandering third instar larvae were harvested and anesthetized by submersion in a drop of glycerol in a chamber that contained a cotton ball soaked by a few drops of ether. Class IV neurons in the dorsal cluster (ddaC neurons) in segments A4-6 were imaged on Zeiss LSM 5 Live with a 40x/1.3 Plan-Neofluar oil immersion objective. A series of tiled Z-stack images were captured and assembled by the Zeiss software package to reconstruct the entire dendritic field of ddaC neurons. Maximum intensity projections were then generated from Z-stack images.

Testing the effects of *tiptop*

It has been recently reported that VDRC 2nd-generation RNAi strains have an unexpected confound (Green et al., 2014) in which some insertions cause unintended overexpression of the *tiptop* (*tio*) gene. To test for this confounding effect, we performed a PCR validation for positive hits from the VDRC 2nd-generation library and found that only one insensitive candidate line (KK106169) and three hypersensitive candidate lines (KK100312, KK108683 and KK105905) possess the transgene integration at the annotated site that is predicted to cause overexpression of *tio* gene (Table S2). Two other hypersensitive candidates showed inconclusive PCR results, which might be accompanied by an integration and/or rearrangement of the annotated integration site (Table S2). If *tio* overexpression on its own were to cause a non-specific nociception phenotype we would expect to observe defective nociception phenotypes in a higher fraction of lines from the KK collection. Thus, the nociception phenotypes in majority of our hits from the KK collection cannot be explained by unintended *tio* expression. PCR for detection of KK lines that may affect expression of *tiptop* were performed as previously described (Green et al., 2014). In addition, we found no effect of overexpressing of tio on dendrite morphogenesis (Figure S2).